Hindawi
Advances in Materials Science and Engineering
Volume 2020, Article ID 4732683, 13 pages
https://doi.org/10.1155/2020/4732683

Research Article

Evolution of Dynamic Recrystallization in 5CrNiMoV Steel during Hot Forming

Zhiqiang Hu and Kaikun Wang

School of Materials Science and Engineering, University of Science and Technology Beijing, Beijing 100083, China

Correspondence should be addressed to Kaikun Wang; kkwang@mater.ustb.edu.cn

Received 31 May 2019; Revised 30 October 2019; Accepted 21 November 2019; Published 9 January 2020

Academic Editor: Michael J. Schütze

Copyright © 2020 Zhiqiang Hu and Kaikun Wang. This is an open access article distributed under the Creative Commons Attribution License, which permits unrestricted use, distribution, and reproduction in any medium, provided the original work is properly cited.

The dynamic recrystallization (DRX) behavior of 5CrNiMoV steel was investigated through hot compression at temperatures of 830–1230°C and strain rates of 0.001–10 s^{-1}. From the experimental results, most true stress-strain curves showed the typical nature of DRX that a single peak was reached at low strains followed by a decrease of stress and a steady state finally at relatively high strains. The constitutive behavior of 5CrNiMoV steel was analyzed to deduce the operative deformation mechanisms, and the correlation between flow stress, temperature, and strain rate was expressed as a sine hyperbolic type constitutive equation. Based on the study of characteristic stresses and strains on the true stress-strain curves, a DRX kinetics model was constructed to characterize the influence of true strain, temperature, and strain rate on DRX evolution, which revealed that higher temperatures and lower strain rates had a favorable influence on improving the DRX volume fraction at the same true strain. Microstructure observations indicated that DRX was the main mechanism and austenite grains could be greatly refined by reducing the temperature of hot deformation or increasing the strain rate when complete recrystallization occurred. Furthermore, a DRX grain size model of 5CrNiMoV was obtained to predict the average DRX grain size during hot forming.

1. Introduction

Hot work die steel is a kind of metal material widely used for forging dies, hot extrusion dies, and die-casting dies, which makes the metal heated above the recrystallization temperature or the liquid metal into a workpiece. On account of the strict property requirements in the course of serving, it is necessary to precisely control the microstructure in the forging process. In order to get the optimum microstructure in terms of properties, such as strength, ductility, impact toughness, and thermal stability, the deformation process parameters such as temperature, strain per pass, strain rate, and initial grain size must be well selected. When the metal is subjected to plastic deformation at high temperature larger than half melting temperature, dynamic recrystallization (DRX) is the main approach of microstructure control and mechanical property improvement [1–4]. Therefore, detailed research on the DRX behavior of metals during hot working is essential to optimizing processing parameters.

Considerable investigations have been done on DRX kinetics, and those research studies concentrate on revealing the relationships between the deformation conditions and the microstructures by analyzing the true strain-stress curves obtained from hot compression tests. Recrystallization models were constructed based on the hot compression tests with wide temperature and strain rate ranges to predict DRX evolution [5–8]. For a more accurate dynamic recrystallization model, it was of great importance to obtain the critical conditions for DRX, which was usually identified by using the $\theta - \sigma$ and $(d\theta/d\sigma) - \sigma$ curves [9–11]. Wu and Han [12] presented a kinetics model, and a third-order polynomial expression was fitted to determine the critical condition for the onset of dynamic recrystallization. Gan et al. [13] structured the kinetics equations of DRX and a constitutive model to predict the flow stress behavior, of which fifth order

polynomial fitting and nonlinear curve fitting were, respectively, presented for determining the critical strain and extrapolating work hardening stress. The research studies not only estimated the recrystallized volume fraction and grain size based on DRX models but also compared the calculated results with the experimental values [14, 15]. These investigations fully verified the accuracy of the DRX models in predicating DRX evolution, as well as its wide applicability. Besides, Luo et al. [16] analyzed the dynamic recrystallization (DRX) behavior of the AFA alloy under different deformation conditions by combining techniques of electron back-scattered diffraction (EBSD) and transmission electron microscopy (TEM), and the results showed that the nucleation mechanisms of DRX mainly included the strain-induced grain boundary (GB) migration, grain fragmentation, and subgrain coalescence. Aashranth et al. [17] proposed a novel technique, known as flow softening index (FSI), to assess DRX, and found that FSI values were associated with the grain growth, intermediate FSI values associated with DRX, and high FSI values associated with the work-hardening and flow localisation phenomena. These new analytical methods also played an important role in the qualitative or semiquantitative study of dynamic recrystallization during hot deformation.

5CrNiMoV steel is a die steel mainly used for making all kinds of large forging dies. Although 5CrNiMoV steel has been widely used in industrial applications, the hot deformation process of the steel has been less investigated and only little information on the dynamic recrystallization (DRX) behavior or flow stress behavior of the steel has been reported. So far, the influence of annealing, forging state, and quenching tempering state on the microstructures of steel matrix composites (SMCs) with 5CrNiMo steel as matrix was investigated by the metallographic analysis method [18]. The changes in strength, hardness, and impact ductility of 5CrNiMo steel after the addition of different contents of RE La element were investigated [19]. Besides, activation energies for plastic deformation of the low alloy steel Din 56CrNiMoV7 (5CrNiMoV) were studied using tensile tests in the temperature range 660–800°C [20]. To supplement the research on the forming property of hot work die steel 5CrNiMoV, the present study explored the DRX behavior and microstructure evolution at different deformation conditions based on the isothermal hot compression tests. And a constitutive equation, a DRX model, and a DRX grain size model were constructed to predict the DRX evolution.

2. Materials and Methods

The 5CrNiMoV steel used in this research, with a chemical composition (wt.%) of 0.54C - 0.25Si - 0.72Mn - 0.012P - 0.003S - 0.96Cr - 1.58Ni - 0.36Mo - 0.074 V - (bal.)Fe, was sampled from a 15 t large forged die. Cylindrical specimens for hot compression tests with a diameter of 10 mm and a height of 15 mm were machined. The prior austenite microstructure of the water-cooled samples after holding at 1230°C for 180 s is revealed in Figure 1(a). Single-pass thermosimulation compression experiments were carried out with a Gleeble 3500 thermomechanical simulator, according to the process illustrated in Figure 1(b). During the process, argon was used to protect the specimens from surface oxidation. Tantalum foil and high-temperature lubricate were used between the anvils and the specimens to reduce the friction. The specimens were heated to 1230°C at a heating rate of $10^{\circ}C \cdot s^{-1}$ and held for 3 min and then cooled to the experiment temperature at the cooling rate of $10^{\circ}C \cdot s^{-1}$. Then, the specimens were held at the forming temperature for 30 s to get a uniform temperature distribution. The compression experiments were performed at strain rates of 0.001, 0.01, 0.1, 1, and $10\ s^{-1}$, at temperatures of 830, 930, 1030, 1130, and 1230°C, respectively, to a maximum true strain of 0.8. After deformation, the specimens were immediately quenched in water to preserve the final deformed microstructure. The quenched specimens were sliced along the axial section. The sections were polished and etched in a solution of picric acid (5 g) + H_2O (100 ml) + HCl (2 ml) + benzene sulfonic acid (2 g) at 50°C for 3-4 min. Then, the optical micrographs were recorded in the centre region of the samples using a metalloscope, and the average recrystallized grain size of specimens was measured using the software Image-Pro Plus, according to the line interception method described in ASTM E112-96 standards.

3. Result and Discussion

3.1. Analysis of True Stress-Strain. The typical true stress-strain curves were obtained at different strain rates and temperatures, as shown in Figure 2. The flow stress was significantly influenced by forming temperature, strain rate, and true strain. Generally, as the true strain increased, the true stress increased almost perpendicularly during the initial stage and then slowly increased to a peak stress, before finally dropping to a relatively steady state [21]. As seen from Figure 2(a), at a given deformation temperature of 1230°C, the flow stress increased with the increase of the strain rate. At the strain rates of $0.001\ s^{-1}$, $0.01\ s^{-1}$, and $0.1\ s^{-1}$, the flow curves showed a single peak followed by a decrease of stress and finally reached a plateau, which implied the occurrence of the full dynamic recrystallization (DRX) phenomenon [22, 23]. At the strain rates of $1\ s^{-1}$ and $10\ s^{-1}$, the flow curves showed dynamic recovery (DRV) character without a peak stress. However, DRX was previously observed in deformed samples whose flow curves showed no strongly defined peak. As seen from Figure 2(b), at the same strain rate of $0.1\ s^{-1}$, the flow stress decreased with the increase of deformation temperature. All the true stress-strain curves demonstrated work hardening with a maximum in the flow stress followed by softening, and the peak flow stress and the strain at flow curves decreased as the test temperature increased. It was due to the fact that the increase of deformation temperature increased the rate of the vacancy diffusion, cross-slip of screw dislocations, and climb of edge dislocations. Besides, large hot work dies were generally forged at high temperature and relatively low strain rate, and DRX was the prime softening mechanism for hot work die steel 5CrNiMoV at the evaluated conditions.

3.2. The Constitutive Behavior. Zener and Hollomon discovered that true stress-strain relationship not only

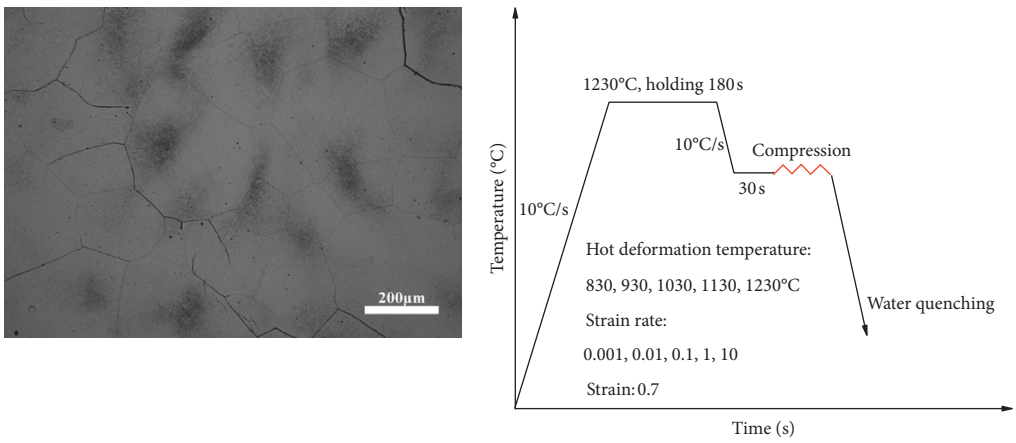

Figure 1: (a) The prior austenite grains of as-received 5CrNiMoV steel. (b) Schematic diagram of hot compression test.

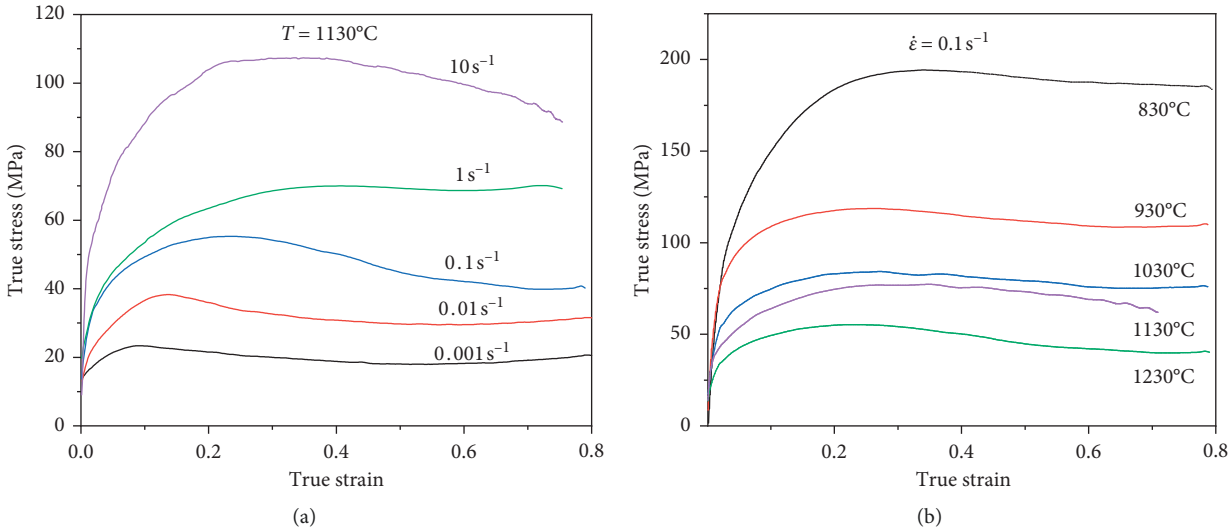

Figure 2: Typical true stress-strain curves of hot work die steel 5CrNiMoV at different deformation conditions.

depended on the chemical composition but also relied on the material deformation temperature and strain rate. They introduced Zener–Hollomon parameter Z, also known as the temperature compensated strain rate [24], to consider the effects of true strain, deformation temperature, and strain rate on the deformation behaviors. The relationship among the flow stress, the deformation temperature, and the strain rate in the plastic deformation process of metallic materials can be expressed by

$$Z = \dot{\varepsilon} \exp\left(\frac{Q_{act}}{RT}\right) = A(\sinh(\alpha\sigma))^n, \quad (1)$$

where $\dot{\varepsilon}$ is strain rate (s^{-1}), σ is the true stress (MPa) (usually taken as the peak stress), R is the universal gas constant (8.314 J/(mol.K)), T is the absolute temperature (K), Q_{act} is the activation energy of deformation (J/mol), and A, α, and n are constants independent of temperature. The value of α was determined through serial computation to be 0.0128 using $\alpha = \beta/n_1$, where n_1 was obtained by linear fitting $\ln\dot{\varepsilon}$ and $\ln\sigma$ (Figure 3(a)) and β was the average slope of $\ln\dot{\varepsilon}$ versus σ (Figure 3(b)).

To obtain the activation energy Q_{act} and material constants A and n, the natural logarithm of both sides of equation (1) was taken, and it is shown in the following equation:

$$\ln\dot{\varepsilon} = \ln A + n\ln(\sinh(\alpha\sigma)) - \frac{Q_{act}}{RT}. \quad (2)$$

When the temperature (T) was constant, material constant n was expressed as follows, with relevant straight lines for different conditions shown in Figure 3(c):

$$n = \left[\frac{\partial\ln\dot{\varepsilon}}{\partial(\ln(\sinh(\alpha\sigma)))}\right]_T. \quad (3)$$

The activation energy Q_{act} indicated the natural deformation ability of steel and was calculated as follows, with relevant straight lines at different conditions shown in Figure 3(d):

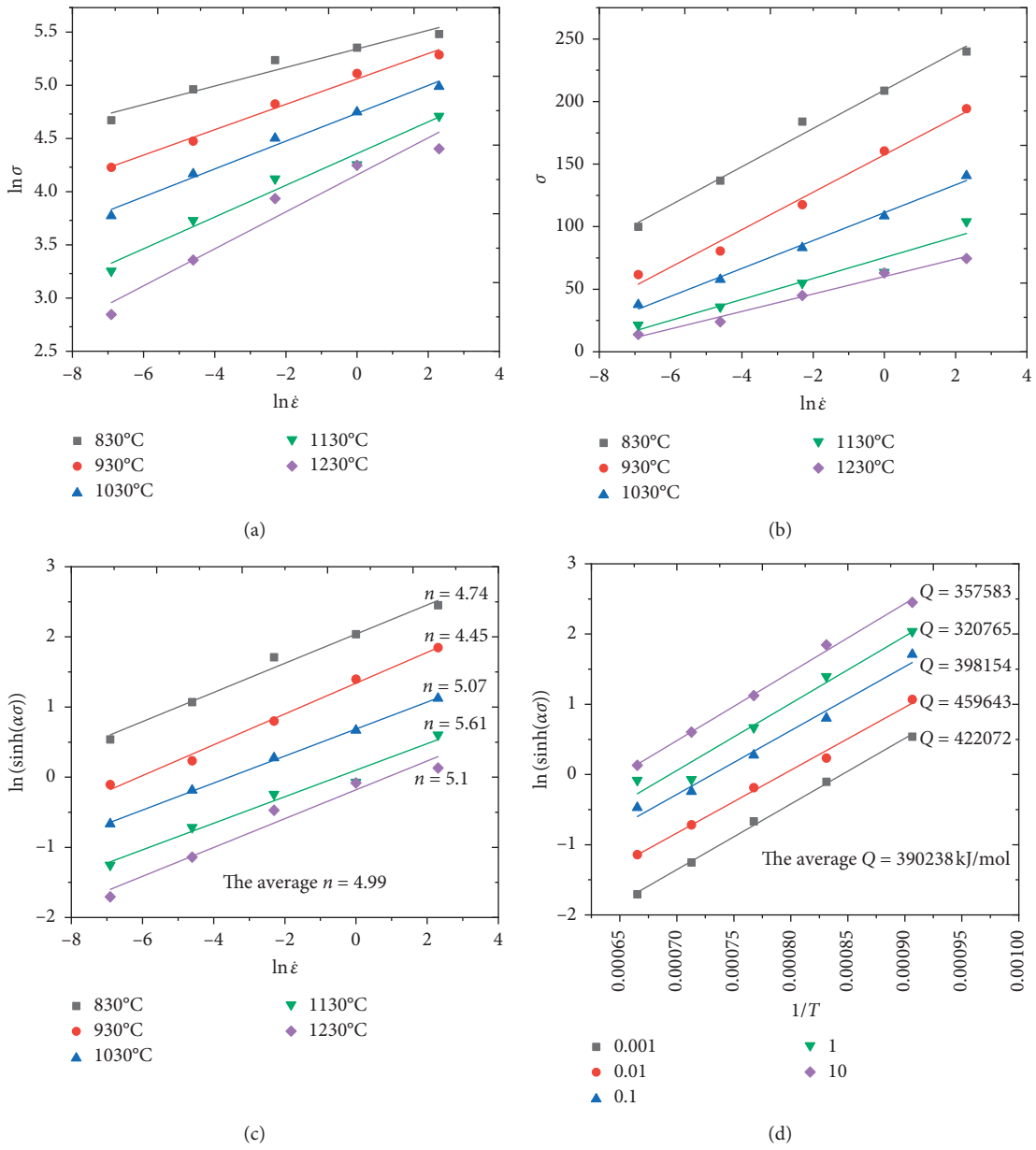

Figure 3: Relationships between (a) $\ln \dot{\varepsilon}$ and $\ln \sigma$, (b) $\ln \dot{\varepsilon}$ and σ, (c) $\ln \dot{\varepsilon}$ and $\ln(\sinh(\alpha\sigma))$, and (d) $\ln(\sinh(\alpha\sigma))$ and $1/T$.

$$Q_{\text{act}} = R * n * \left[\frac{\partial(\ln(\sinh(\alpha\sigma)))}{\partial(1/T)}\right]_{\dot{\varepsilon}}. \quad (4)$$

The average activation energy Q_{act} and material constant n were determined as 390.238 kJ/mol and 4.927, respectively. As was known that the average activation energy Q was used to describe the required energy to reach, such as the peak point of flow curve and the occurrence of DRX, it could be the activation energy for DRV, DRX, or a combination of them with other phenomena such as dynamic precipitation and their corresponding microstructural mechanisms. The average activation energy (Q_{d}) for hot deformation was separated into thermal (Q_{th}) and mechanical (Q_{mech}) parts. The thermal activation was found necessary to propel diffusion and help dislocations bypass the short-range barriers such as the solute atoms. The mechanical energy could help dislocations overcome strong long-range obstacles such as dislocation tangles [25]. Assuming Q_{th} was constant and equal to the activation energy for diffusion (Q_{dif}), Q_{th} of 5CrNiMoV steel was calculated as 322.86 kJ/mol according to the empirical formula [26]. The acquired average apparent activation energy Q of 5CrNiMoV steel at different deformation was 390.238 kJ/mol, and the average mechanical energy (Q_{mech}) was about 67.378 kJ/mol. For the existence of the mechanical energy (Q_{mech}), which depends on the applied stress and therefore varies with the deformation temperature and strain rate (Figure 3(d)), the apparent activation energy is often much larger than any imagined atomic mechanism [27]. For example, the linear regression of the data resulted in the values of $Q = 435.3$ and 374 kJ/mol

for the VCN200 and AISI 4135 steel compressed at the same deformation condition. It was revealed that the different apparent activation energies were attributed to about 30% difference between the carbon equivalents of the steel [28].

Besides, according to equation (3), the value of n was constant with strain rate. As shown in Figure 3(c), it was observed that the value of n for 5CrNiMoV steel presented a rising trend on the whole with temperature rising, which was probably for the increase in rate of DRX with temperature increasing. Many investigations indicated that this difference stemmed from the dissimilar dynamic softening mechanisms of the materials [25, 29]. The average value of material constant n was exactly close to 5, which indicated that the deformation mechanism was mainly controlled by the glide and climb of dislocations. Moreover, to be proposed as an index to the microstructural evolutions, it showed that the deformation mechanism was discontinuous dynamic recrystallization (DDRX). Besides, the peak stress points have been used to find the regression n values after the initiation of DRX, which could lead to a little decrease in value of n from the theoretical value of 5 to 4.927 [30, 31]. The Zener–Hollomon parameter for this steel was expressed as follows:

$$Z = \dot{\varepsilon} \exp\left(\frac{390238}{RT}\right). \tag{5}$$

Besides, another material constant A was calculated to be 7.405×10^{13}, which was obtained by plotting $\ln Z$ versus $\ln(\sinh(\alpha\sigma))$ at different deformation conditions, as shown in Figure 4. In summary, substituting the constants Q, A, α, and n into equation (1), the constitutive equation for hot work die steel 5CrNiMoV could be expressed as

$$\dot{\varepsilon} = 1.17 \times 10^{14} (\sinh(0.0128\sigma))^{4.927} \cdot \exp\left(-\frac{390238}{RT}\right). \tag{6}$$

Furthermore, the constitutive equation of flow stress can be written as

$$\begin{cases} \sigma = \dfrac{1}{0.0128} \ln\left\{\left(\dfrac{Z}{1.17 \times 10^{14}}\right)^{1/4.927} \right. \\ \qquad \left. + \left[\left(\dfrac{Z}{1.17 \times 10^{14}}\right)^{2/4.927} + 1\right]^{1/2}\right\}, \\ Z = \dot{\varepsilon} \exp\left(\dfrac{390238}{8.314T}\right). \end{cases} \tag{7}$$

3.3. Dynamic Recrystallization Kinetics. In the hot forging process, dislocation continually increased and accumulated with the increasing deformation amount. When it reached a critical value, DRX nuclei would form and grow up near grain boundaries, twin boundaries, and deformation bands. Once recrystallization occurred in the region, the dislocation density of it would reduce by rearrangement and annihilation of dislocation [32]. The peak stress-strain, critical stress-strain, steady-state stress, and saturated stress on the true stress-strain curve

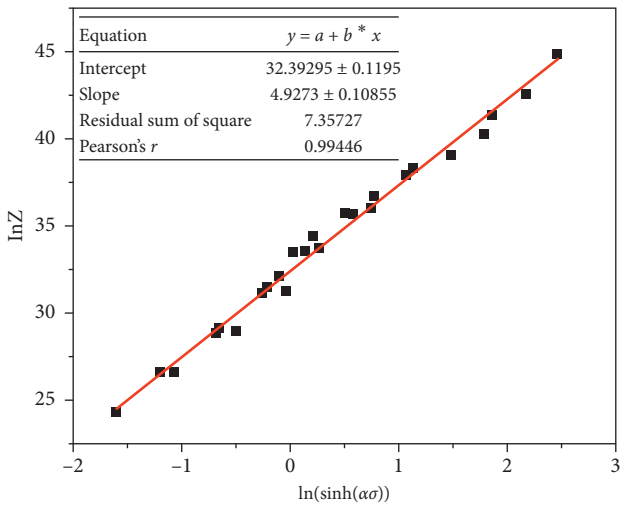

Figure 4: Relationships between $\ln Z$ and $\ln(\sinh(\alpha\sigma))$.

are illustrated in Figure 5(a). Here, the uppermost curve (σ_{sat}) is regarded as resulting from the operation of dynamic recovery alone. It represents the assumed work-hardening behavior of the un-recrystallized regions and can be derived from the work-hardening behavior prior to the critical strain (ε_c). The critical strain (ε_c) for DRX depends on the composition of the material, grain size prior to deformation, and deformation condition (temperature and strain rate). DRX is initiated at the critical strain (ε_c) and critical stress (σ_c) after which it leads to more and more softening and is responsible for the difference between the DRV and DRX curves [33, 34]. The onset of DRX can be recognized by an inflection point in the curve of work-hardening rate (θ, $\theta = \partial\sigma/\partial\varepsilon$) versus flow stress ($\sigma$). This method eliminates the need for extrapolated flow stress data, and these critical points can be precisely located on the flow curves. Typical work-hardening curve at temperature 1230°C and strain rate 0.1 s^{-1} is shown in Figure 5(b), from which it was easy to determine the values of the steady stress (σ_s) and the saturation stress (σ_{sat}) of DRV, the critical stress (σ_c) and the peak stress (σ_p) of DRX, and the corresponding critical strain (ε_c) and peak strain (ε_p) of DRX. With the method described above, characteristic stresses and strains at different deformation conditions were obtained and are shown in Table 1.

The Avrami model is frequently used to evaluate the kinetics of crystallization and growth of lipids. However, it is difficult to apply to the entire range of the crystallization event, mainly because the rate of crystallization and the dimensionality of growth in the model are assumed to be linear and constant according to the assumptions [35, 36]. It is generally admitted that DRX follows Avrami's law, and the most common expression to quantitatively interpret this phenomenon is expressed as equation (8). It was used to predict recrystallized fraction for strains greater than ε_c due to the effect of dynamic recrystallization. And the value of X_{DRX} should be equal to one when the steady state was reached.

$$X_{DRX} = 1 - \exp\left[-k_d\left(\frac{\varepsilon - \varepsilon_c}{\varepsilon_p}\right)^{n_d}\right], \quad \varepsilon \geq \varepsilon_c, \tag{8}$$

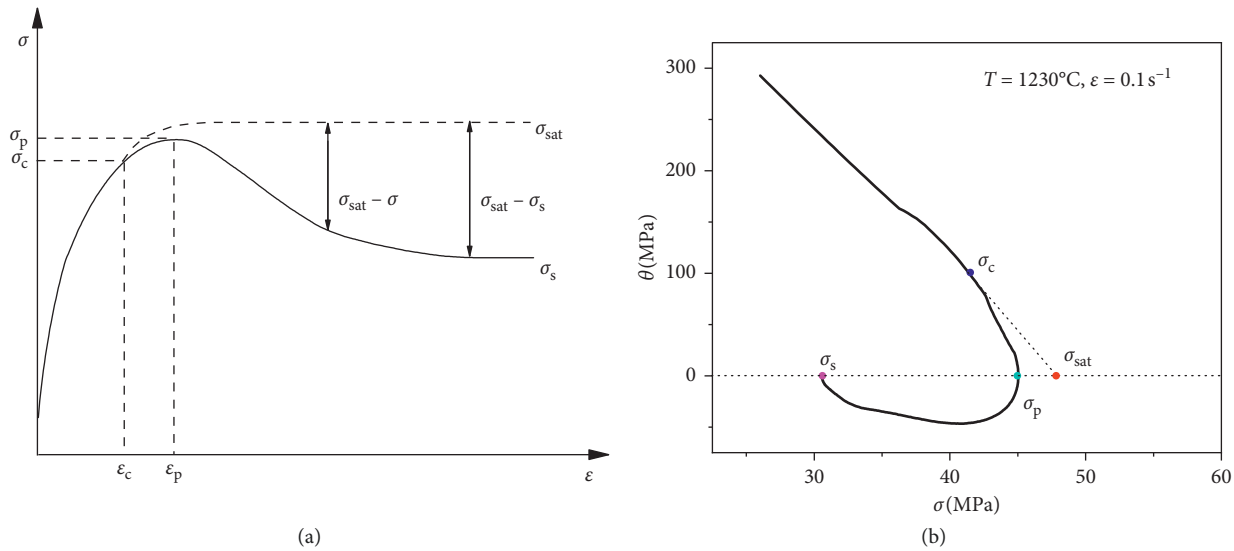

Figure 5: (a) Schematic plot showing the peak stress-strain, critical stress-strain, steady-state stress, and saturated stress on the true stress-strain curve. (b) Work-hardening rate with respect to stress: determination of σ_c, σ_{sat}, σ_p, and σ_s.

Table 1: Values of characteristic strains and stresses at different deformation conditions.

T (°C)	$\dot{\varepsilon}$ (s^{-1})	σ_p (MPa)	ε_p (MPa)	σ_c (MPa)	ε_c (MPa)	σ_s (MPa)	σ_{sat} (MPa)
930	0.001	63.60	0.256	62.33	0.187	56.55	65.3
930	0.01	81.70	0.263	78.55	0.192	68.8	85.2
930	0.1	118.65	0.373	116.57	0.272	108.48	119.8
1030	0.001	39.00	0.121	36.06	0.073	29.27	42.6
1030	0.01	57.87	0.181	56.44	0.147	44.81	59.7
1030	0.1	83.98	0.25	82.36	0.181	75.05	85.8
1130	0.001	23.31	0.084	22.41	0.065	17.98	24.3
1130	0.01	38.21	0.13	36.20	0.096	29.52	40.4
1130	0.1	55.27	0.242	53.88	0.165	40.23	56.3
1230	0.001	15.65	0.064	14.80	0.046	11.42	16.7
1230	0.01	26.44	0.108	25.37	0.075	17.92	27.2
1230	0.1	45.04	0.172	44.54	0.148	30.56	45.7

where X_{DRX} is the DRX volume fraction, k_d and n_d are the material constants, and ε_c and ε_p are the critical strain and peak strain, respectively. This expression, which is modified from the Avrami' equation, means that X_{DRX} depends on the strain and other deformation conditions [37]. The value of X_{DRX} was determined from the flow-curve analysis. The method for determining X_{DRX} by analyzing the flow stress curves is illustrated in Figure 5(a). The following expression was adopted to determine the DRX volume fraction:

$$X_{DRX} = \frac{\sigma_{sat} - \sigma}{\sigma_{sat} - \sigma_s}, \tag{9}$$

where σ_{sat} denotes the flow stress and its softening effect that only results from dynamic recovery (without DRX), σ_s is the steady-state stress under the DRX conditions, and σ is the true stress. Substituting characteristic stresses at different deformation conditions into equation (9), X_{DRX} was obtained. Taking the logarithm of both sides of the expression, we get the following:

$$\ln\left(-\ln\left(1 - X_{DRX}\right)\right) = \ln k_d + n_d \ln\left(\frac{\varepsilon - \varepsilon_c}{\varepsilon_p}\right). \tag{10}$$

As shown in Figure 6, the material constants at different deformation conditions were ascertained through the linear regression analysis. However, the material parameters under different deformation conditions differed greatly. It is known that k_d and n_d are not constants and clearly depend on the temperature, strain rate, and the chemical composition of the steel [35]. To improve the accuracy of the model, they were described as a function of Z. Figure 7 shows the plots of the parameters $\ln n_d$ and $\ln k_d$ versus $\ln Z$. An approximate linear relationship between $\ln n_d$ and $\ln Z$ and $\ln k_d$ and $\ln Z$ was observed. More often, the value of n_d and k_d declined with increase in Z, and the value of Z depended on the deformation condition. As was known that increasing temperature or decreasing strain rate gave rise to the increase of Z therefore leads to the increase of X_{DRX}. It was indicated that the two parameters n_d and k_d depended on the deformation temperature and strain rate. In other words, the two parameters showed an impact on the recrystallization volume fraction. By regression analysis, the dependences of n_d and k_d were expressed as follows:

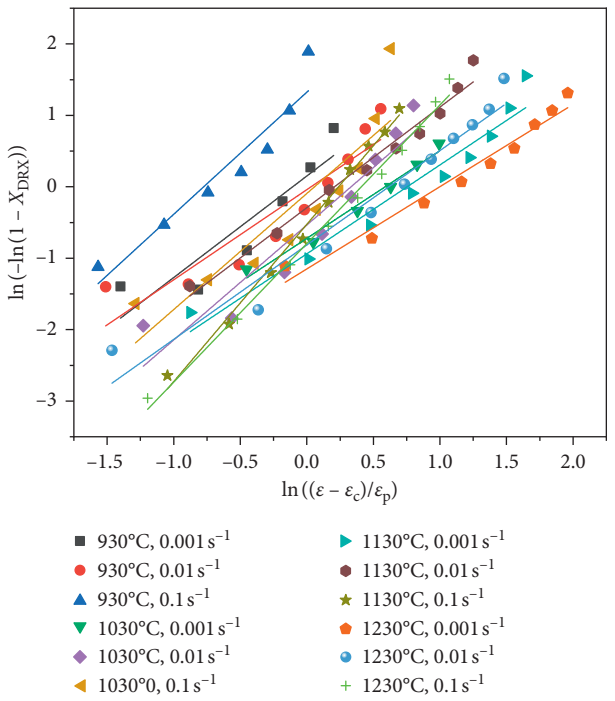

FIGURE 6: Relationships between $\ln(-\ln(1 - X_{DRX}))$ and $\ln((\varepsilon_c - \varepsilon)/\varepsilon_p)$ at different deformation conditions.

$$\begin{cases} n_d = 0.536Z^{0.032}, \\ k_d = 0.0235Z^{0.1056}. \end{cases} \tag{11}$$

Deformation temperature and strain rate had an appreciable impact on the critical strain and the peak strain. For each of the DRX characteristic true stress-strain curves, a critical strain and a peak strain were obtained [13]. Furthermore, the relationships between the peak strain and the deformation conditions and the critical strain and the deformation conditions can be, respectively, expressed as the exponential function of the Zener–Hollomon parameter. Figure 8 shows the plots $\ln \varepsilon_p$ and $\ln \varepsilon_c$ versus $\ln Z$. By linear fitting, relevant material parameters were obtained and the dependences ε_p of and ε_c on Z were written as follows:

$$\begin{aligned} \varepsilon_p &= 0.002335Z^{0.14057}, \\ \varepsilon_c &= 0.00166Z^{0.14144}. \end{aligned} \tag{12}$$

Besides, the relationship between ε_p and ε_c can be usually described as follows:

$$\varepsilon_c = C\varepsilon_p, \tag{13}$$

where C is the constant. The value of material constant C was usually between 0.3 and 0.9, which had been previously reported for steel. By substituting the values of ε_p and ε_c into equation (13) and regression analysis (Figure 9), the value of C was calculated to be 0.727, and the relationship between ε_p and ε_c was expressed as

$$\varepsilon_c = 0.727\varepsilon_p. \tag{14}$$

Until now, all the parameters needed for the determination of X_{DRX} have been obtained or expressed as functions

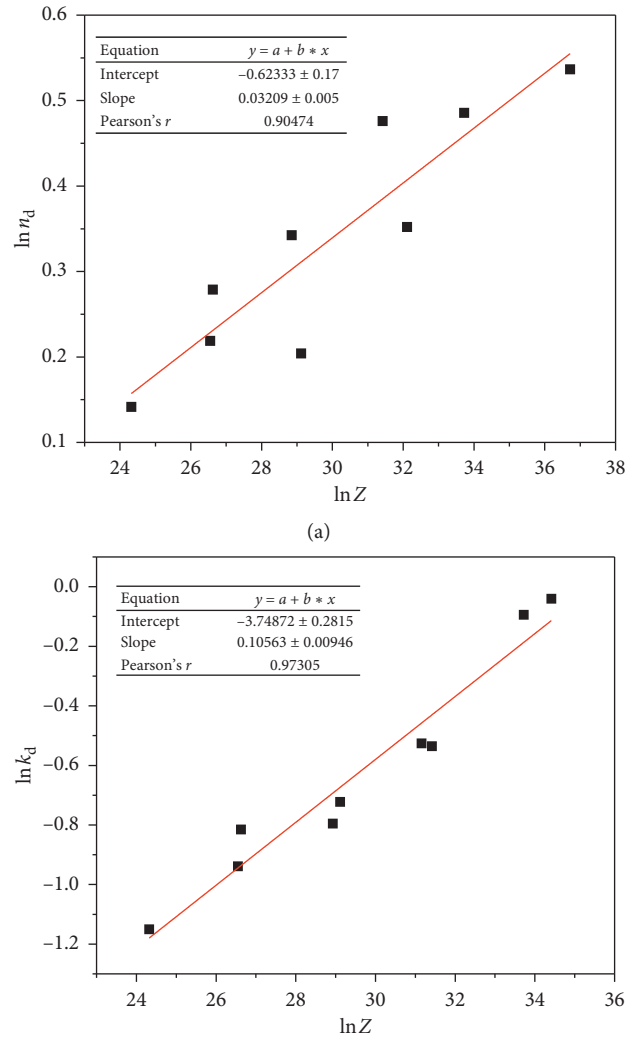

FIGURE 7: Relationships between (a) $\ln n_d$ and $\ln Z$ and (b) $\ln k_d$ and $\ln Z$.

of Zener–Hollomon parameter. Finally, the kinematic model of DRX of 5CrNiMoV steel can be expressed as follows:

$$\begin{cases} X_{DRX} = 1 - \exp\left[-k_d\left(\dfrac{\varepsilon - \varepsilon_c}{\varepsilon_p}\right)^{n_d}\right], \quad \varepsilon \geq \varepsilon_c, \\ n_d = 0.536Z^{0.032}, \\ k_d = 0.0235Z^{0.1056}, \\ \varepsilon_p = 0.002335Z^{0.14057}, \\ \varepsilon_c = 0.00166Z^{0.14144}, \\ Z = \dot{\varepsilon}\exp\left(\dfrac{390238}{8.314T}\right). \end{cases} \tag{15}$$

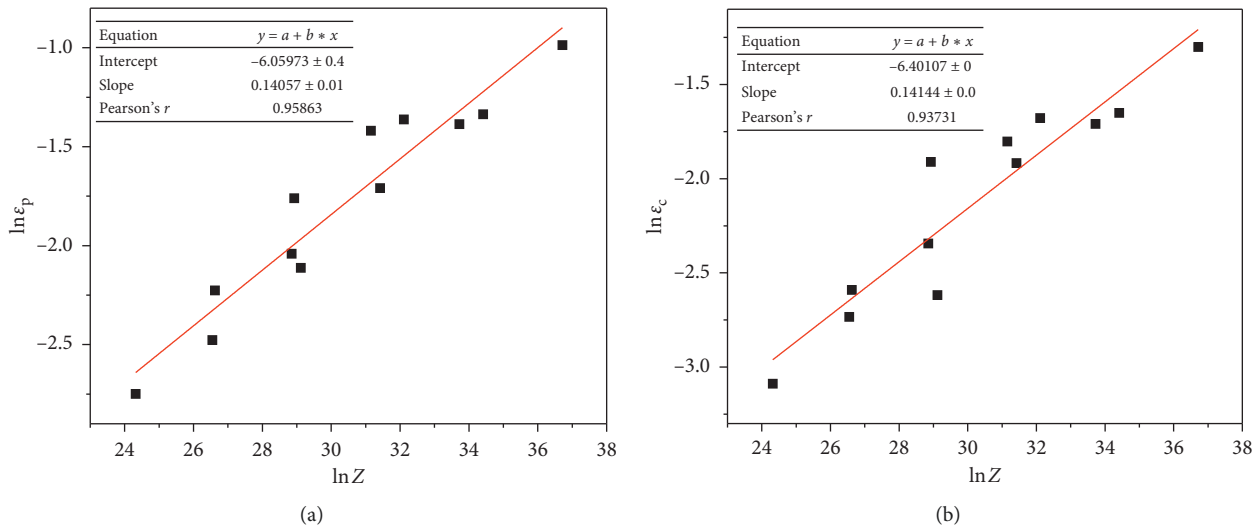

Figure 8: Relationships between (a) $\ln \varepsilon_p$ and $\ln Z$ and (b) $\ln \varepsilon_c$ and $\ln Z$.

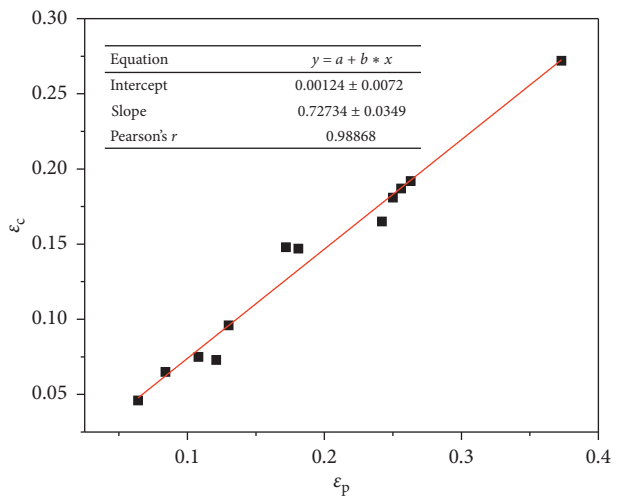

Figure 9: Relationships between ε_p and ε_c.

3.4. Microstructure Observations. The optimal metallography has been selected to observe microstructure evolution. Figures 10(a)–10(e) show the microstructure of 5CrNiMoV steel deformed at a constant temperature of 830°C and strain rates of 0.001, 0.01, 0.1, 1, and 1 s^{-1}. The red arrows in Figure 10 illustrate the new recrystallized DRX grains. It should be noticed that DRX grain size decreased evidently with increasing strain rate, as it enhanced both the work-hardening rate and dislocation density, thereby producing more nuclei per unit volume and the energy stored. However, at the strain rate of 0.1, 1, and 10 s^{-1}, DRX behavior stayed incomplete and the unrecrystallization grains are illustrated in Figure 10 by the white arrows. It was for that higher strain rates, to some extent, brought less time for the movements of grain boundaries and dislocations, which restrained the growth of DRX nuclei [38, 39].

Figures 11(a)–11(e) show the microstructure of 5CrNiMoV steel deformed at a constant strain rate of 1 s^{-1} and the temperature of 830, 930, 1030, 1130, and 1230°C. The red and white arrows in Figure 11 illustrate the new recrystallized DRX grains and un-recrystallized grains, respectively. At the temperature of 830°C, there were still un-recrystallized grains. As the temperature was increased to 930°C, many elongated grains disappeared, and the microstructure was gradually replaced by fine DRX grains. For the increased deformation temperature of 1030, 1130, and 1230°C, growth of the grains turned to be easier. As shown in Figures 11(c)–11(e), big grains were formed and tiny grains between the grain boundaries were observed, which indicated the growth of recrystallized grains. It was pointed that because recrystallization activation energy increased with deformation temperature, dislocation motion and crystal slip were promoted, which enhanced grain-boundary migration, facilitating nucleation and growth of DRX grains [40]. In summary, although it was possible to cause incomplete recrystallization by reducing the temperature of hot deformation or increasing the strain rate, it showed favorable impact on grain refinement when complete recrystallization occurred.

It was observed that the complete DRX grain size usually increased with the increases of the deformation temperature or the decreases of the strain rate. The average dynamic recrystallization grain size of 5CrNiMoV steel at different deformation conditions was measured by the quantitative metallography method according to the ASTM standard. The measured results are listed in Table 2. The average grain size of dynamic recrystallization depended on the deformation temperature and the strain rate. It can be expressed as follows:

$$D_{DRX} = a_3 \dot{\varepsilon}^{m_3} \exp\left[\frac{Q_3}{RT}\right], \tag{16}$$

where D_{DRX} denotes the average grain size of dynamic recrystallization (μm), Q_3 is the activation energy for grain growth (J/mol), $\dot{\varepsilon}$ is the strain rate (s^{-1}), T is the deformation temperature (K), R is the gas constant (8.314 J/(mol.K)), and

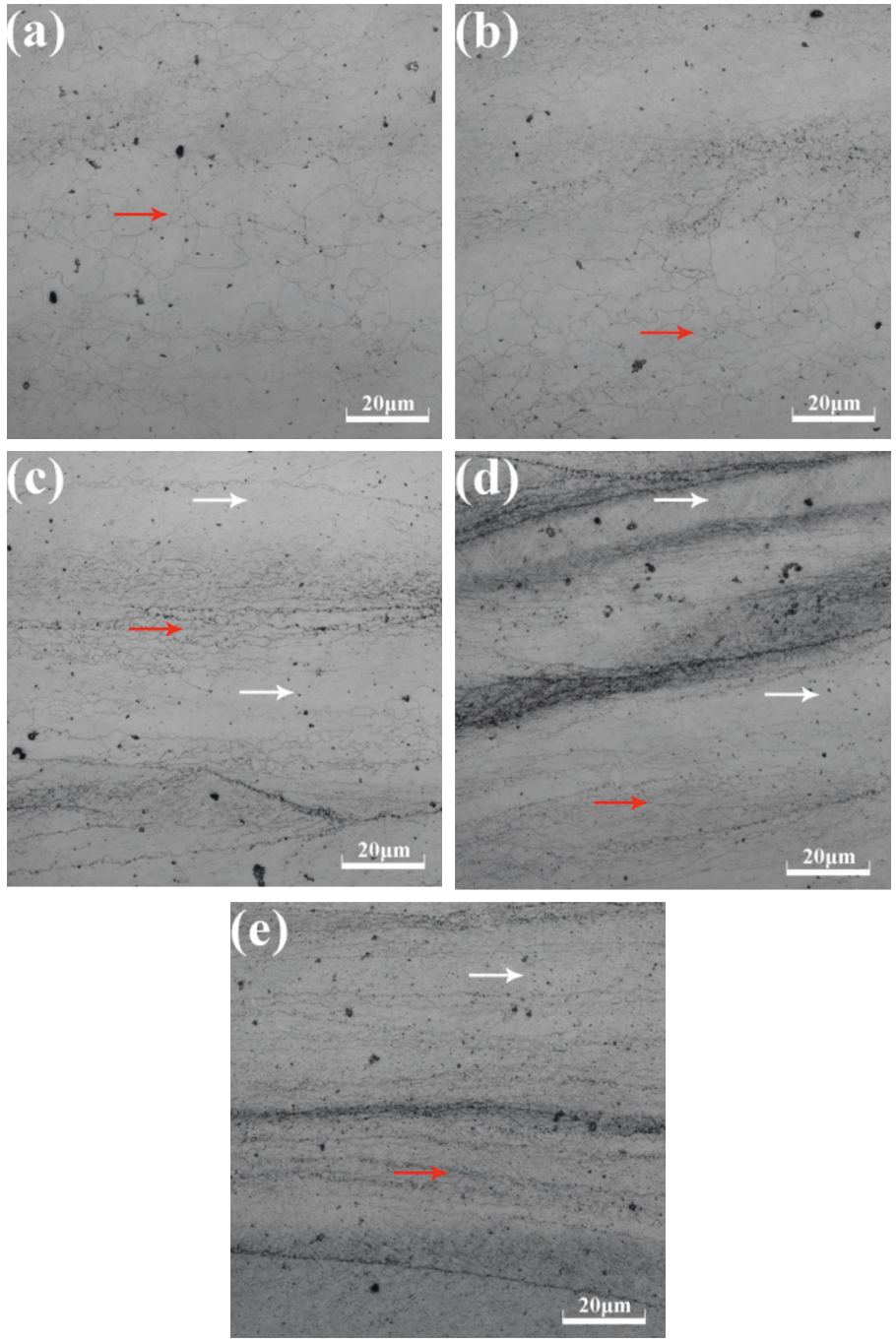

FIGURE 10: Optical microstructure of 5CrNiMoV steel deformed at the temperature of 830°C: (a) $\dot{\varepsilon} = 0.001\ s^{-1}$, (b) $\dot{\varepsilon} = 0.01\ s^{-1}$, (c) $\dot{\varepsilon} = 0.1\ s^{-1}$, (d) $\dot{\varepsilon} = 1\ s^{-1}$, and (e) $\dot{\varepsilon} = 10\ s^{-1}$.

a_3 and m_3 are the material constants. Taking the natural logarithm of both sides of equation (16), we get the following:

$$\ln D_{DRX} = \ln a_3 + m_3 \ln \dot{\varepsilon} + \frac{Q_3}{RT}. \tag{17}$$

Through the linear regression analysis of $\ln D_{DRX}$ versus $\ln \dot{\varepsilon}$(Figure 12(a)) and $\ln D_{DRX}$ versus $1/T$ (Figure 12(b)) respectively, the values were as follows: $m_3 = -0.1674$ and $Q_3 = -102593$ J/mol. After determining the material parameters m_3 and Q_3, a_3 was obtained as 173,488 from the relationships between D_{DRX} and $\dot{\varepsilon}^{m_3} \exp[Q_3/RT]$ (Figure 13). The model of dynamic recrystallization grain size of 5CrNiMoV steel can be expressed as follows:

$$D_{DRX} = 173488\dot{\varepsilon}^{-0.1674} \exp\left[\frac{-102.594 \times 10^3}{RT}\right]. \tag{18}$$

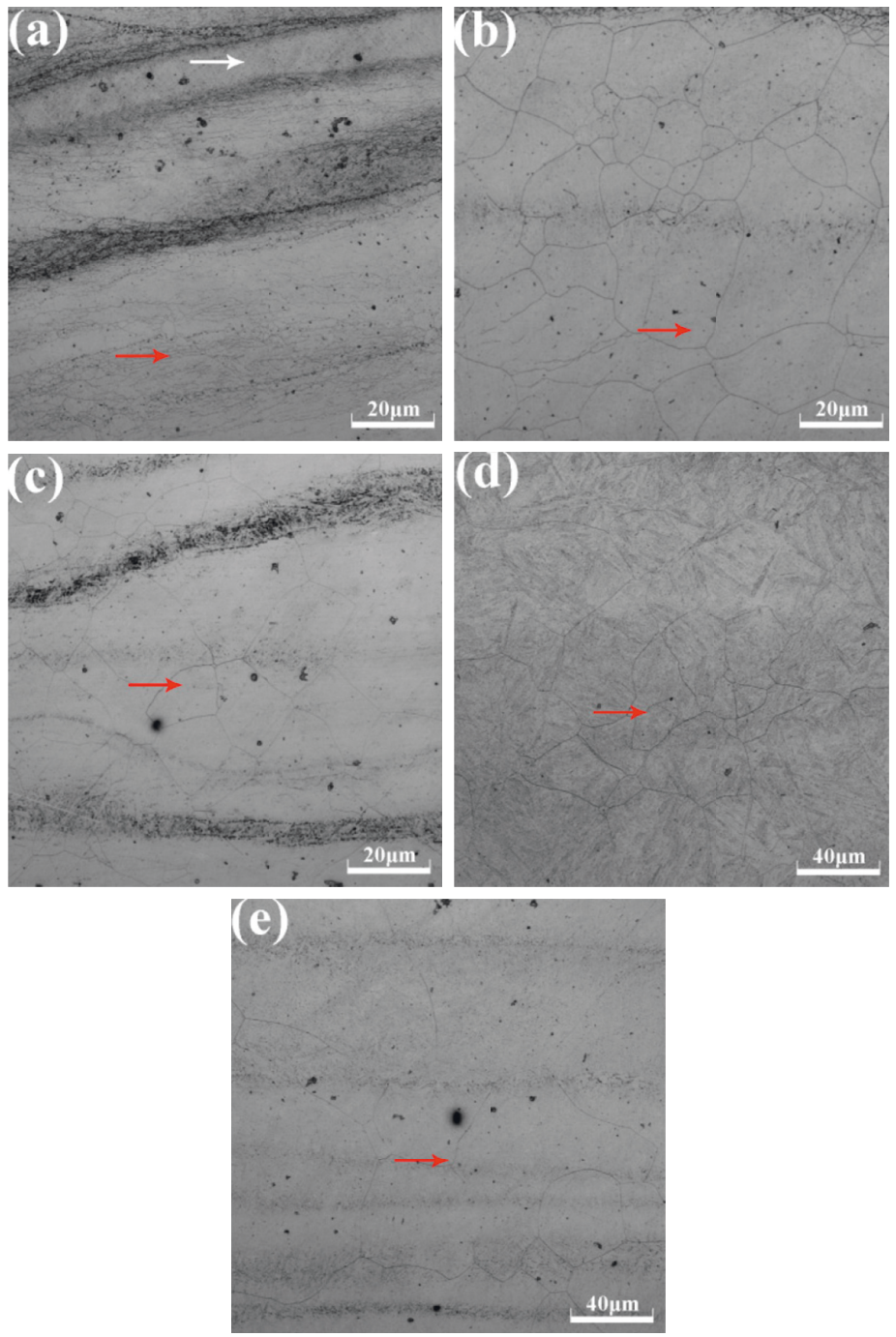

Figure 11: Optical microstructure of 5CrNiMoV steel deformed at the strain rate of $1\,s^{-1}$: (a) $T = 830^{\circ}C$, (b) $T = 930^{\circ}C$, (c) $T = 1030^{\circ}C$, (d) $T = 1130^{\circ}C$, and (e) $T = 1230^{\circ}C$.

Table 2: Average dynamic recrystallization grain size (μm).

Temperature (°C)	$0.001\,s^{-1}$	$0.01\,s^{-1}$	$0.1\,s^{-1}$	$1\,s^{-1}$	$10\,s^{-1}$
830	6.75	5.51	3.71	2.25	1.85
930	20.98	14.18	9.69	6.68	4.36
1030	42.83	27.86	20.23	13.23	9.49
1130	83.53	55.67	38.85	26.31	18.87
1230	149.20	98.21	70.30	46.24	33.94

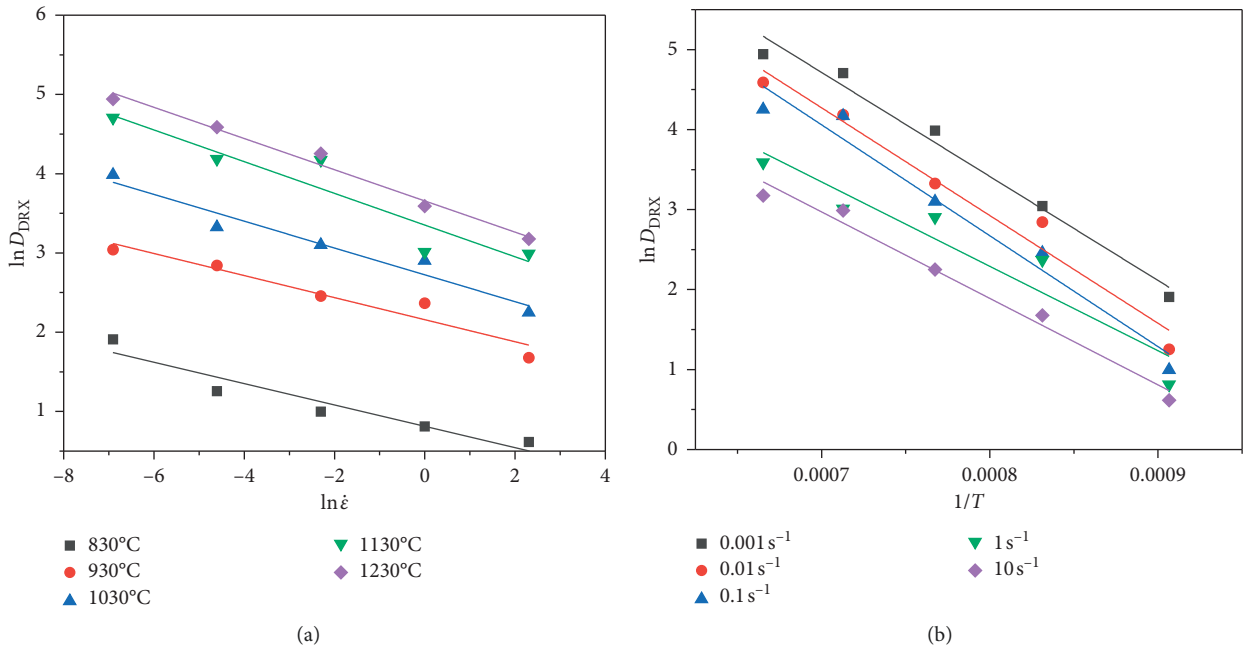

Figure 12: Relationships between (a) $\ln D_{DRX}$ and $\ln \dot{\varepsilon}$ and (b) $\ln D_{DRX}$ and $1/T$.

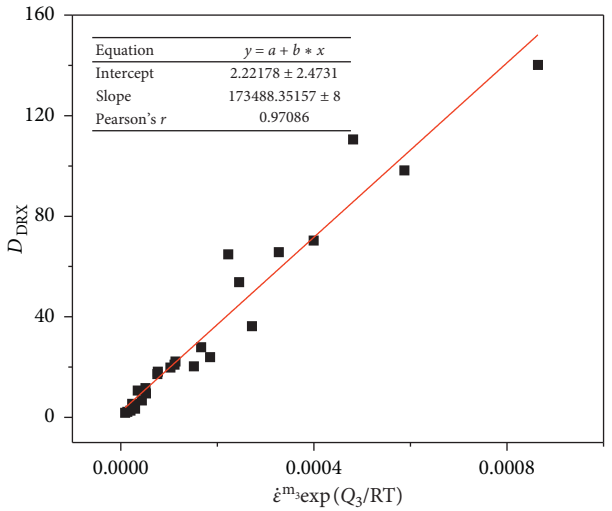

Figure 13: Relationships between D_{DRX} and $\dot{\varepsilon}^{m_3}\exp(Q_3/RT)$.

4. Conclusion

Based on the isothermal compression tests on the Gleeble 3500 thermal simulator in the range of temperatures 830, 930, 1030, 1130, and 1230°C and strain rates 0.001, 0.01, 0.1, 1, and 10 s^{-1}, the dynamic recrystallization (DRX) kinetics of 5CrNiMoV steel was investigated. The following conclusions were drawn from the present study:

(1) True stress-strain curves obtained by hot compression tests exhibited the typical characteristics of dynamic recovery or dynamic recrystallization. The temperature and strain rate had significant influences on the true stress which increased with decreasing deformation temperature and increasing strain rate. The constitutive behavior of 5CrNiMoV steel was analyzed to deduce the operative deformation mechanisms. Its apparent activation energy Q (390.238 kJ/mol) was larger than that calculated based on the empirical formula for the lattice self-diffusion in 5CrNiMoV steel. The value of material constant n was exactly close to 5, which indicated that the deformation mechanism was mainly controlled by the glide and climb of dislocations. By further analysis of true stress-strain curves, the Arrhenius-type constitutive equation with Zener–Hollomon parameter for the steel was constructed as follows:

$$\begin{cases} \sigma = \dfrac{1}{0.0128}\ln\left\{\left(\dfrac{Z}{1.17\times10^{14}}\right)^{1/4.927} + \left[\left(\dfrac{Z}{1.17\times10^{14}}\right)^{2/4.927}+1\right]^{1/2}\right\}, \\ Z = \dot{\varepsilon}\exp\left(\dfrac{390238}{8.314T}\right). \end{cases} \quad (19)$$

(2) Characteristic stresses and strains on the true stress-strain curves at different deformation conditions were obtained, and the dependences of the critical strain, peak strain, and materials constant k_d and n_d on the Zener–Hollomon parameter were investigated. To quantitatively analyze the impact of the strain and other deformation conditions on the DRX volume fraction, a modified model from the Avrami' equation was established as follows:

$$\begin{cases} X_{\mathrm{DRX}} = 1 - \exp\left[-k_{\mathrm{d}}\left(\dfrac{\varepsilon - \varepsilon_{\mathrm{c}}}{\varepsilon_{\mathrm{p}}}\right)^{n_{\mathrm{d}}}\right], \quad \varepsilon \geq \varepsilon_{\mathrm{c}}, \\ n_{\mathrm{d}} = 0.536Z^{0.032}, \\ k_{\mathrm{d}} = 0.0235Z^{0.1056}, \\ \varepsilon_{\mathrm{p}} = 0.002335Z^{0.14057}, \\ \varepsilon_{\mathrm{c}} = 0.00166Z^{0.14144}, \\ Z = \dot{\varepsilon}\exp\left(\dfrac{390238}{8.314T}\right). \end{cases} \tag{20}$$

(3) Microstructure observations indicated that DRX was the main mechanism of work softening for steels during large deformation and austenite grains were greatly refined by reducing the temperature of hot deformation or increasing the strain rate when complete recrystallization occurred. And the DRX grain size model of 5CrNiMoV steel could be expressed as follows:

$$D_{\mathrm{DRX}} = 173488\dot{\varepsilon}^{-0.1674}\exp\left[\frac{-102.594 \times 10^3}{RT}\right]. \tag{21}$$

Data Availability

The data used to support the findings of this study are included within the article.

Conflicts of Interest

The authors declare that there are no conflicts of interest regarding the publication of this paper.

Acknowledgments

This work was financially supported by the National Key Research and Development Program of China (2017YFB0701803 and 2016YFB0701403) and the State Key Laboratory of Nickel and Cobalt Resources Comprehensive Utilization.

References

[1] B. Shahriari, R. Vafaei, E. M. Sharifi, and K. Farmanesh, "Modeling deformation flow curves and dynamic recrystallization of BA-160 steel during hot compression," *Metals and Materials International*, vol. 24, no. 5, pp. 955–969, 2018.

[2] Y. Wang, Y. Deng, and S. Xiu, "Study on the dynamic recrystallization mechanism during pre-stress dry grinding," *Journal of Manufacturing Processes*, vol. 32, pp. 100–109, 2018.

[3] Y. Xu, C. Chen, X. Zhang, H. Dai, J. Jia, and Z. Bai, "Dynamic recrystallization kinetics and microstructure evolution of an AZ91D magnesium alloy during hot compression," *Materials Characterization*, vol. 145, pp. 39–52, 2018.

[4] H. Zhou, H. Zhang, J. Liu, S. Qin, and Y. Lv, "Prediction of flow stresses for a typical nickel-based superalloy during hot deformation based on dynamic recrystallization kinetic equation," *Rare Metal Materials and Engineering*, vol. 47, no. 11, pp. 3329–3337, 2018.

[5] Y. Sun, R. Wang, J. Ren, C. Peng, and Y. Feng, "Hot deformation behavior of Mg-8Li-3Al-2Zn-0.2Zr alloy based on constitutive analysis, dynamic recrystallization kinetics, and processing map," *Mechanics of Materials*, vol. 131, pp. 158–168, 2019.

[6] L. Chen, W. Sun, J. Lin, G. Zhao, and G. Wang, "Modelling of constitutive relationship, dynamic recrystallization and grain size of 40Cr steel during hot deformation process," *Results in Physics*, vol. 12, pp. 784–792, 2019.

[7] X. Zhong, L. Huang, L. Wang, F. Liu, X. Dong, and Z. Zhang, "A discontinuous dynamic recrystallization model incorporating characteristics of initial microstructure," *Transactions of Nonferrous Metals Society of China*, vol. 28, no. 11, pp. 2294–2306, 2018.

[8] W. Wang, J. Zhao, R. X. Zhai, and R. Ma, "Arrhenius-type constitutive model and dynamic recrystallization behavior of 20Cr2Ni4A alloy carburizing steel," *Steel Research International*, vol. 88, no. 3, Article ID 1600196, 2017.

[9] N. Park, "Precise flow stress analysis for the occurrence of dynamic ferritic transformation and dynamic recrystallization of austenite in low carbon steel," *Korean Journal of Metals and Materials*, vol. 56, no. 11, pp. 779–786, 2018.

[10] G.-z. Quan, Y.-l. Li, L. Zhang, and X. Wang, "Evolution of grain refinement degree induced by dynamic recrystallization for Nimonic 80A during hot compression process and its FEM analysis," *Vacuum*, vol. 139, pp. 51–63, 2017.

[11] Z. C. Sun, H. L. Wu, J. Cao, and Z. K. Yin, "Modeling of continuous dynamic recrystallization of Al-Zn-Cu-Mg alloy during hot deformation based on the internal-state-variable (ISV) method," *International Journal of Plasticity*, vol. 106, pp. 73–87, 2018.

[12] C. Wu and S. Han, "Hot deformation behavior and dynamic recrystallization characteristics in a low-alloy high-strength Ni-Cr-Mo-V steel," *Acta Metallurgica Sinica-English Letters*, vol. 31, no. 9, pp. 963–974, 2018.

[13] B. Gan, M. Zhang, H. Li, Y. Yao, and L. Li, "A modified constitutive model and dynamic recrystallization behavior of high-N Mn18Cr18 alloy," *Steel Research International*, vol. 88, no. 9, Article ID 1600433, 2017.

[14] A. Najafizadeh and J. J. Jonas, "Predicting the critical stress for initiation of dynamic recrystallization," *ISIJ International*, vol. 46, no. 11, pp. 1679–1684, 2006.

[15] Q. Yang, C. Ji, and M. Zhu, "Modeling of the dynamic recrystallization kinetics of a continuous casting slab under heavy reduction," *Metallurgical and Materials Transactions A-Physical Metallurgy and Materials Science*, vol. 50, no. 1, pp. 357–376, 2019.

[16] R. Luo, Q. Zheng, J. Zhu et al., "Dynamic recrystallization behavior of Fe-20Cr-30Ni-0.6Nb-2Al-Mo alloy," *Rare Metals*, vol. 38, no. 2, pp. 181–188, 2019.

[17] B. Aashranth, D. Samantaray, S. Kumar et al., "Flow softening index for assessment of dynamic recrystallization in an austenitic stainless steel," *Journal of Materials Engineering and Performance*, vol. 26, no. 7, pp. 3531–3547, 2017.

[18] N. Zhang, Y. Qiang, C. Zhang, and G. Ding, "Microstructure and property of WC/steel matrix composites," *Emerging Materials Research*, vol. 4, no. 2, pp. 149–156, 2015.

[19] H. Guo, X. Hao, and Z. He, "Effect of RE La element on the mechanical properties of 5CrNiMo forging die steel," *Journal*

of University of Science and Technology Beijing, vol. 29, no. 12, pp. 1209–1211, 2007.

[20] A. S. E. Brito and A. P. Loureiro, "Activation energies for plastic deformation of the low alloy steel din 56CrNiMoV7 in the temperature range 660–800°C," in *Strength of Metals and Alloys (ICSMA 8)*, P. O. Kettunen, T. K. Lepisto, and M. E. Lehtonen, Eds., pp. 1025–1030, Elsevier, Amsterdam, Netherlands, 1988.

[21] X. Wang, K. Chandrashekhara, S. N. Lekakh, D. C. Van Aken, and R. J. O'Malley, "Modeling and simulation of dynamic recrystallization behavior in alloyed steel 15V38 during hot rolling," *Steel Research International*, vol. 90, no. 4, Article ID 1700565, 2019.

[22] A. R. Salehi, S. Serajzadeh, and N. Yazdipour, "A study on flow behavior of A-286 superalloy during hot deformation," *Materials Chemistry and Physics*, vol. 101, no. 1, pp. 153–157, 2007.

[23] Y. F. Xia, S. Long, T. Wang, and J. Zhao, "A study at the workability of ultra-high strength steel sheet by processing maps on the basis of DMM," *High Temperature Materials and Processes*, vol. 36, no. 7, pp. 657–667, 2017.

[24] M. J. Luton and C. M. Sellars, "Dynamic recrystallization in nickel and nickel-iron alloys during high temperature deformation," *Acta Metallurgica*, vol. 17, no. 8, pp. 1033–1043, 1969.

[25] A. Momeni, "The physical interpretation of the activation energy for hot deformation of Ni and Ni-30Cu alloys," *Journal of Materials Research*, vol. 31, no. 8, pp. 1077–1084, 2016.

[26] A. A. Vasilyev, S. F. Sokolov, N. G. Kolbasnikov, and D. F. Sokolov, "Effect of alloying on the self-diffusion activation energy in γ-iron," *Physics of the Solid State*, vol. 53, no. 11, pp. 2194–2200, 2011.

[27] J. Fu, F. Li, and Y. Li, "Characterization and the improved Arrhenius model of 0Cr11Ni2MoVNb steel during hot deformation process," *IOP Conference Series: Materials Science and Engineering*, vol. 382, p. 022027, 2018.

[28] A. Momeni and S. M. Abbasi, "On the opposition of dynamic recrystallization and solute dragging in steels," *Journal of Alloys and Compounds*, vol. 622, pp. 318–326, 2015.

[29] G. R. Ebrahimi, A. Momeni, S. M. Abbasi, and H. Monajatizadeh, "Constitutive analysis and processing map for hot working of a Ni-Cu alloy," *Metals and Materials International*, vol. 19, no. 1, pp. 11–17, 2013.

[30] H. Mirzadeh, "Quantification of the strengthening effect of reinforcements during hot deformation of aluminum-based composites," *Materials & Design (1980–2015)*, vol. 65, pp. 80–82, 2015.

[31] H. Mirzadeh, "Constitutive analysis of Mg-Al-Zn magnesium alloys during hot deformation," *Mechanics of Materials*, vol. 77, pp. 80–85, 2014.

[32] A. Hermant, E. Suzon, P. Petit et al., "Hot deformation and recrystallization mechanisms in a coarse-grained, niobium stabilized austenitic stainless steel (316Nb)," *Metallurgical and Materials Transactions A*, vol. 50, no. 4, pp. 1625–1642, 2019.

[33] A. Saboori, M. Pavese, S. Biamino, P. Fino, and M. Lombardi, "Determination of critical condition for initiation of dynamic recrystallisation in Zr-1%Nb alloy," *Journal of Alloys and Compounds*, vol. 757, pp. 1–7, 2018.

[34] H. Mirzadeh and A. Najafizadeh, "Prediction of the critical conditions for initiation of dynamic recrystallization," *Materials & Design*, vol. 31, no. 3, pp. 1174–1179, 2010.

[35] S. F. Medina and C. A. Hernandez, "Modelling of the dynamic recrystallization of austenite in low alloy and microalloyed steels," *Acta Materialia*, vol. 44, no. 1, pp. 165–171, 1996.

[36] C. A. Hernandez, S. F. Medina, and J. Ruiz, "Modelling austenite flow curves in low alloy and microalloyed steels," *Acta Materialia*, vol. 44, no. 1, pp. 155–163, 1996.

[37] G. Quan, Y. Shi, Y. Wang, B. Kang, T. Ku, and W. Song, "Constitutive modeling for the dynamic recrystallization evolution of AZ80 magnesium alloy based on stress-strain data," *Materials Science and Engineering A*, vol. 528, no. 28, pp. 8051–8059, 2011.

[38] Y. Yang, T. R. Li, T. Jia, Z. D. Wang, and R. D. K. Misra, "Dynamic recrystallization and flow behavior in low carbon Nb-Ti microalloyed steel," *Steel Research International*, vol. 89, no. 4, Article ID 1700395, 2018.

[39] Z. Xiao, Y. Huang, and Y. Liu, "Evolution of dynamic recrystallization in 35CrMo steel during hot deformation," *Journal of Materials Engineering and Performance*, vol. 27, no. 3, pp. 924–932, 2018.

[40] Y. Cheng, H. Du, Y. Wei, L. Hou, and B. Liu, "Metadynamic recrystallization behavior and workability characteristics of HR3C austenitic heat-resistant stainless steel with processing map," *Journal of Materials Processing Technology*, vol. 235, pp. 134–142, 2016.


The Scientific
World Journal
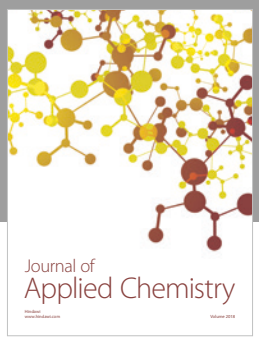
Journal of
Applied Chemistry
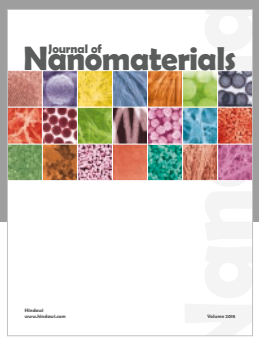
Journal of
Nanomaterials

Scientifica

International Journal of
Polymer Science
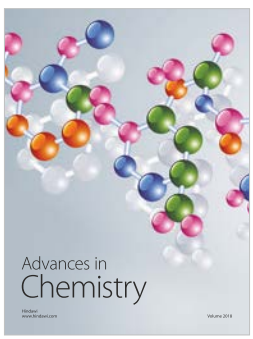
Advances in
Chemistry

Hindawi
Submit your manuscripts at
www.hindawi.com
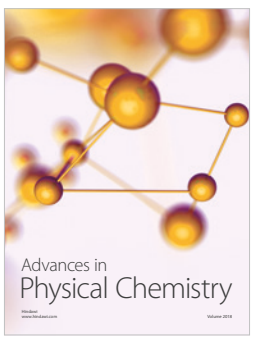
Advances in
Physical Chemistry

International Journal of
Analytical Chemistry
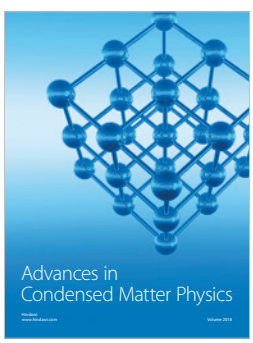
Advances in
Condensed Matter Physics
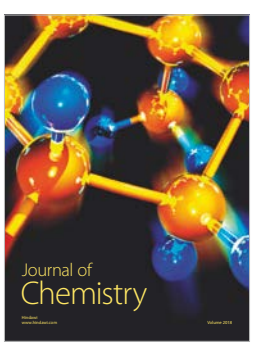
Journal of
Chemistry

International Journal of
Biomaterials
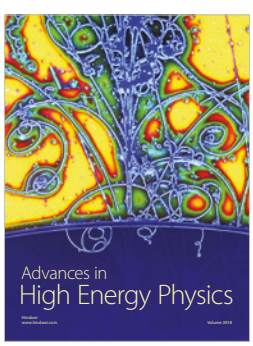
Advances in
High Energy Physics

Journal of
Engineering

Journal of
Nanotechnology

International Journal of
Corrosion

Journal of
Materials

BioMed
Research International
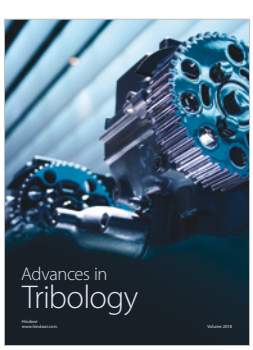
Advances in
Tribology
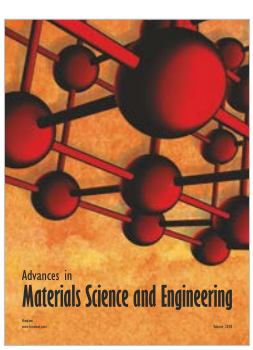
Advances in
Materials Science and Engineering